A multiscale computational framework for wear prediction in knee replacement implants

Yan Li* and Chi Ma

Thayer School of Engineering Dartmouth College, Hanover, NH 03755, U.S.A

Abstract

Wear damage represents a long-term material failure that affects the service life of joint implants. Prediction of wear in bearing inserts under arbitrary joint kinematics and kinetics holds an important key to improving the performance of entire joint implant device through new material development and customized geometry design. In this work, a hierarchical multiscale computational framework that predicts the wear rate of ultra-high molecular weight polyethylene (UHMWPE) insert by resolving the microstructure details and microscale deformation mechanisms is developed. A fully dynamic finite element simulation is carried out at the macroscale level to reproduce the interactions between femoral component and UHMWPE insert according to the knee simulator input profiles. The stress evolution history from the initial wear site is extracted and applied back to the representative volume element (RVE) to further study the microscale deformation mechanisms that are related to wear damage. Activation of different slip systems in the crystalline phase as well as the interplay between the crystalline phase and amorphous phase are captured through a semi-crystal plasticity model. Results shown that improving wear resistance requires minimizing the plastic deformation upon the same external loading while maintaining a load-sharing balance between the crystalline phase and the amorphous phase. A combination of high crystallinity, well-dispersed crystallite with small size and texture alignment along the axial load direction can promote activation of chain pull slip that leads to improved wear resistance.

Keywords: Wear prediction, Ultra-high molecular weight polyethylene (UHMWPE), Crystal plasticity, Knee replacement implants

^{*} Corresponding Author: yan.li@dartmouth.edu

1. Introduction

Artificial joint, also known as prosthesis, is a device that is surgically implanted to replace a natural bone to correct joint abnormalities and to improve joint function (Carr and Goswami, 2009). A typical knee artificial joint, as illustrated in Fig. 1(a), includes a femoral component, a tibial plate and a bearing insert in between. During the walking process, the bearing insert is subjected to cyclic rolling and sliding, as well as the vertical force from body weight as shown in Fig.1(b). Wear debris starts to initiate on the contact surface of bearing insert over a certain number of cycles (Sanders et al., 2016). It has been reported that wear debris not only induces inflammation that leads to patient pain, but can also cause bone tissue damage, implant loosening, and even complete device failure (Callaghan et al., 2004; Nich and Goodman, 2014; Suñer et al., 2012).

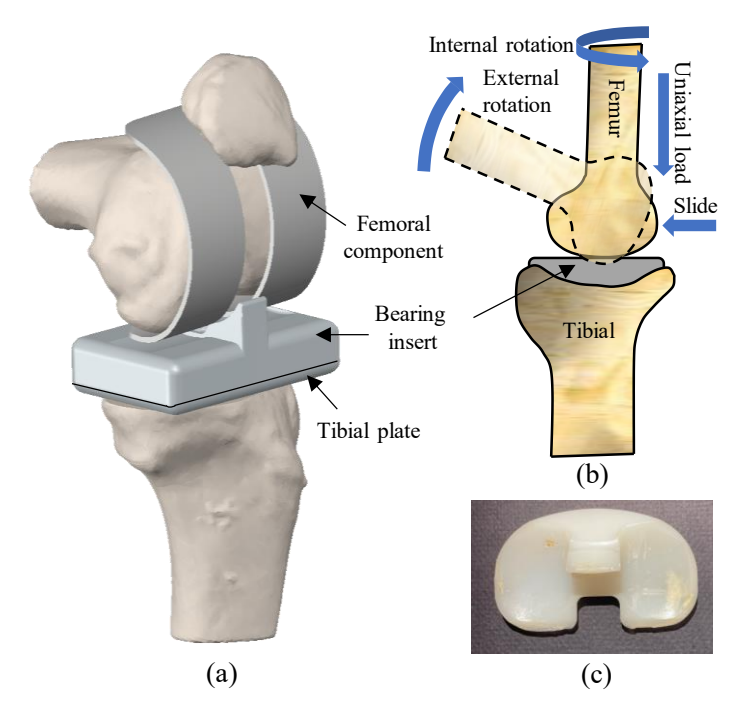


Fig.1 Scheme of (a) a knee artificial joint and (b) loading conditions during the walking cycle. (c) Wear damage on a failed bearing insert (Courtesy of Professor Doug Van Citters).

Accurate prediction of wear damage in joint implants is a challenging task. The reason is several-fold. First, wear is a long-term failure mode that occurs in the order of millions of cycles (McEwen et al., 2005). The actual wear behavior largely depends on the joint kinematics and kinetics that can vary significantly between patients according to each individual's walking gait, weight and types of daily activities, etc. In-depth understanding of wear evolution as function of complex loading history requires large datasets that are impossible to get from experiment alone due to the high cost and long cycles (Knight et al., 2007). Second, existing computational models, although can complement wear

experimentation by accounting for arbitrary prosthesis geometries, kinematics and material selections with higher efficiency and lower cost, cannot realistically reproduce the wear process. Ishikawa et al. (Ishikawa et al., 1996) developed a 2D finite element model to evaluate the pressure distribution on the polyethylene surface at various points during the gait cycle. Contact stress distribution was calculated from elasto-plastic indentation analysis of both femoral and tibial components. Sathasivam et al. (Sathasivam and Walker, 1997) first extended the 2D finite element models to 3D to better capture the intricate contact behavior between prosthetic components. Godest et al. (Godest et al., 2002) developed an explicit finite element approach to further extend the static analyses to account for both kinematics and the internal stress evolution within a single analysis. Abdelgaied et al. (Abdelgaied et al., 2011) improved the wear model that was used for metallic materials for more realistic prediction of wear pattern in polymeric bearing materials. In the above-mentioned studies, bearing insert, which is usually made of ultrahigh molecular weight polyethylene (UHMWPE), is modeled as an isotropic material without considering the microstructure details. While it may be possible to consider the properties of UHMWPE isotropically under a monotonic and uniaxial load, its anisotropic behavior cannot be ignored under complex wear loading conditions as illustrated in Fig. 1(b). UHMWPE is a semi-crystalline polymer that consists of both crystalline lamellar phase and amorphous phase. In general, the crystalline phase exhibits significantly higher stiffness than the amorphous phase (Becker et al., 2011; Polińska et al., 2021). It was reported by Polińska et al. (Polińska et al., 2021) that the Young's modulus of polyethylene crystals, which is measured in the normal direction toward the crystalline a-axis at 25°C, is around 4.9 GPa compared to 3 MPa in the amorphous phase. Therefore, crystallinity, which is equivalent to the volume fraction of crystalline phase, can lead to heterogeneous microscale deformation, and in turn affect the overall material strength and wear behavior. Additionally, the orientation and size distribution of crystalline phase also play an important role in activating different microscale deformation mechanisms, such as lamellar separation, tilting, and interlamellar shear, etc (Bowden and Young, 1974; Lin and Argon, 1994). Currently, lack of knowledge about microstructure evolution under arbitrarily predefined loading conditions—as well as the missing linkage between the anisotropy in microscale deformation and macroscale wear behavior, make the computational predictions hard to match the experiment results. It has been reported that the computationally calculated wear rate is approximately 30% lower than the experiment result (Abdelgaied et al., 2011; Zhang et al., 2017).

Third, a few micromechanics models have been developed to account for morphological texture evolution and slip activations that are not captured in the isotropic constitutive models. However, the effect of microstructure on wear behavior has not been reported. Lee et al. (Lee et al., 1993) proposed a rigid-viscoplastic composite model that has a sandwiched aggregate with a planer crystalline phase and an amorphous phase in an infinitely extended space. This pioneering work provides a useful numerical tool to connect texture evolution with macroscale stress-strain response in semi-crystalline polymers. This work neglects the elasticity and pressure sensitivity during the deformation process.

Dommelen et al. (Van Dommelen et al., 2003) extended Lee's model by introducing elasticity to both crystalline and amorphous phases. In their work, the crystalline phase follows anisotropic elastic deformation, while its plastic deformation is governed by the crystallographic slip on a limited number of slip systems through a rate-dependent crystal plasticity model. The elastic and plastic deformation in the amorphous phase are modelled through the generalized neo-Hookean relation and a strain rate insensitive power law relation, respectively. The detailed stiffness and slip strength of the crystalline phase in UHMWPE were provided by Dong et al. (Dong et al., 2018) through systematic molecular dynamic simulations. The above-mentioned studies all pointed out that incorporation of microstructure details of semi-crystalline polymers can provide more realistic representation of their macroscopic deformation behaviors. However, existing conclusions, which primarily considered monotonic uniaxial tension or compression, cannot be directly used to interpret the wear behaviors in UHMWPE insert that is subjected to complex cyclic wear loading conditions. Additionally, microscale modeling alone, although can account for the heterogeneous microstructural details and deformation mechanisms, is computationally expensive and therefore impractical for wear predictions at the structural scale.

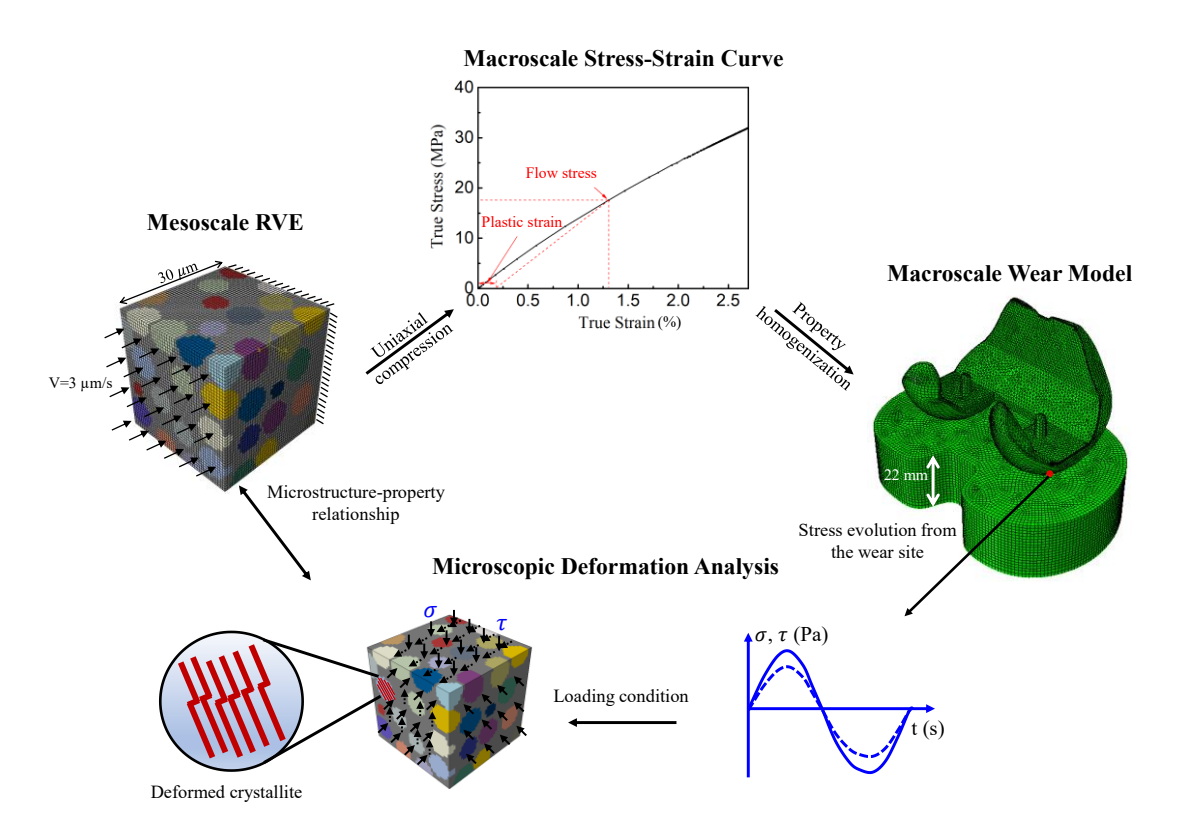


Fig. 2 Computational multiscale framework of wear simulation for implant knee-joint replacement.

In this study, a hierarchical multiscale framework as illustrated in Fig. 2 is developed to predict the wear rate of UHMWPE insert by explicitly accounting for crystallinity,

orientation and size of lamellar crystals. A fully dynamic finite element simulation is carried out at macroscale to reproduce the interactions between femoral component and UHMWPE insert according to the knee simulator input profiles (Abdelgaied et al., 2011). The macroscale constitutive relationship is determined from the representative volume element (RVE) with microstructure information. Wear rate is predicted by calculating the wear volume per cumulative cycles. The stress evolution history from a wear site is extracted and applied back to the RVE to study the texture evolution and slip activations. This framework can provide a comprehensive understanding of wear behavior with reasonable computational cost.

2. Multiscale model description

2.1 Microscale constitutive modeling of the UHMWPE insert

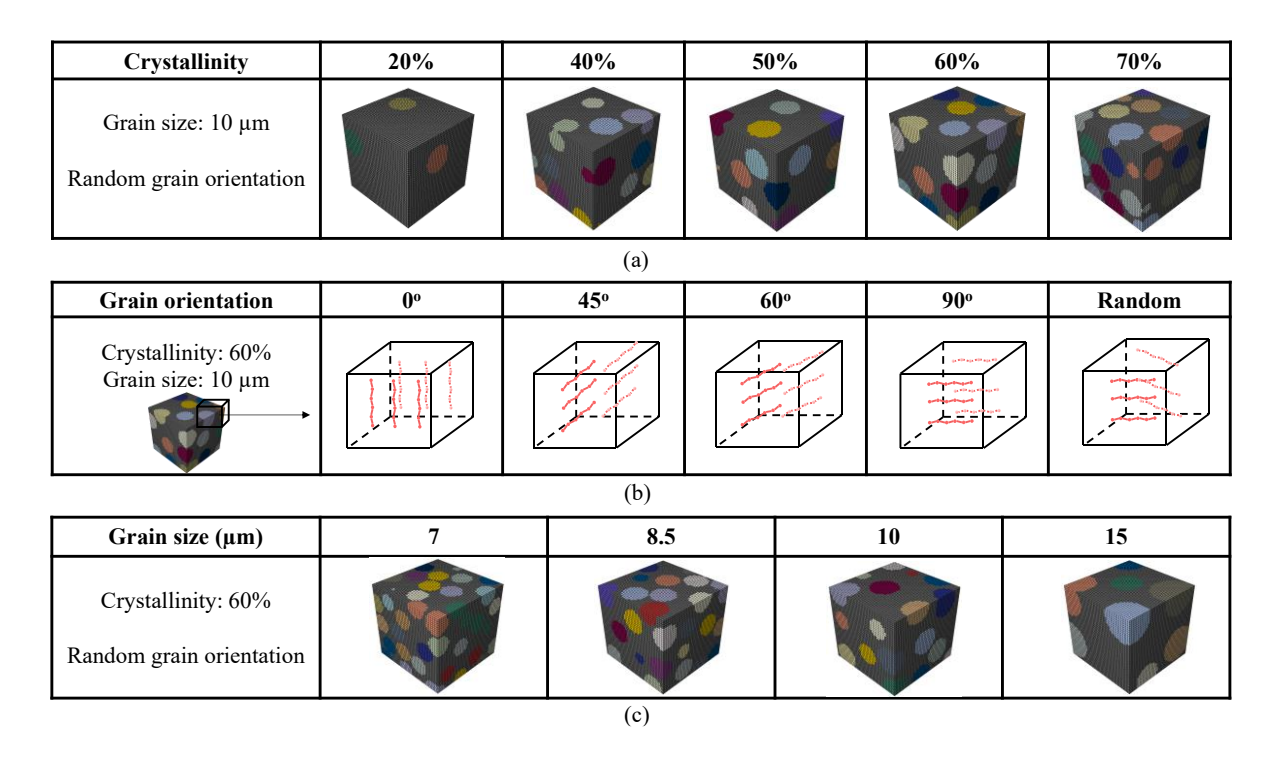


Fig. 3 Computationally generated UHMWPES RVE sets with (a) varied crystallinity, (b) varied crystal grain orientation and (c) varied crystal grain size.

Plastic deformation of UHMWPE is a manifestation of dislocation motion in the crystalline phase, as well as the interactions between the crystalline phase and the amorphous phase. Microscopic details, such as crystallinity, orientation and size of lamellar crystals, largely determine the deformation and wear response by activating different slip systems. Existing macroscopic plasticity models, however, do not account for the microscopic details or the fundamental deformation mechanisms. In this work, three sets of UHMWPE RVEs with randomly distributed uniform circular particles are generated using MATLAB as shown in Fig. 3. In each RVE, the matrix represents the amorphous phase. Its stress-strain response

UHMWPE using traditional cooling technique. Dong et al. (Dong et al., 2018) constructed pure amorphous microstructure and carried out molecular dynamics simulations to evaluate the stress-strain relationship through uniaxial tension and compression. They found that the Young's modulus and activation stress in the amorphous phase are 0.1 GPa and 0.35 MPa, respectively. The detailed constitutive law in Fig. 7 of their work is employed in this study. The elastic-plastic deformation of crystalline phase is modeled using the crystal plasticity (CP) model. The basic premise of CP model is that macroscopic plastic deformation is related to the cumulative process of slip system shearing relative to the lattice. Specifically, the multiplicative decomposition of the total deformation gradient is formulated by

$$\mathbf{F} = \mathbf{F}_{e} \cdot \mathbf{F}_{p}, \tag{1}$$

where \mathbf{F}_e is the elastic deformation gradient representing the elastic stretch and rotation of the crystalline grains, and \mathbf{F}_p is the plastic deformation gradient describing the collective effects of dislocation motion along the active slip planes relative to a fixed lattice in the reference configuration. The resolved shear stress on each slip system is related to the Cauchy stress tensor σ according to

$$\tau^{\alpha} = \mathbf{\sigma}: (\boldsymbol{m}^{\alpha} \otimes \boldsymbol{n}^{\alpha}), \tag{2}$$

where m^{α} and n^{α} denote the slip direction and slip plane normal direction, respectively for the α^{th} slip system. Under the application of resolved shear stress, shearing rate $\dot{\gamma}^{\alpha}$ on the slip systems are related to the plastic velocity gradient L^{p} according to

$$\mathbf{L}^{p} = \dot{\mathbf{F}}_{p} \, \mathbf{F}_{p}^{-1} = \sum_{\alpha=1}^{9} \dot{\gamma}^{\alpha} \, \boldsymbol{m}^{\alpha} \otimes \boldsymbol{n}^{\alpha} \,. \tag{3}$$

The shearing rate $\dot{\gamma}^{\alpha}$ follows the rate-dependent flow rule as

$$\dot{\gamma}^{\alpha} = \dot{\gamma}_0^{\alpha} \left(\frac{\tau^{\alpha}}{D^{\alpha}}\right)^n sign(\tau^{\alpha}), \tag{4}$$

where $\dot{\gamma}_0^{\alpha}$ is the reference shear rate, D^{α} is the drag stress and n is the flow rule exponent. The evolution of drag stress D^{α} is formulated as

$$\dot{D}^{\alpha} = p \left| \dot{\gamma} \right| (q - \frac{D^{\alpha}}{D_0^{\alpha}}), \text{ with } \left| \dot{\gamma} \right| = \sum_{\beta=1}^{9} \left| \dot{\gamma}^{\beta} \right|. \tag{5}$$

Here, D_0^{α} is the initial slip strength as listed in Table 1. Material constants p = 0.005 and q = 1.002 are selected according to Dong et al. (Dong et al., 2018). The plastic velocity gradient \mathbf{L}^p can be obtained by explicitly resolving the shearing rate at each slip system. The updated plastic deformation gradient is computed through backward time integration as

$$\left.\mathbf{F}_{p}^{-1}\right|_{t+1} = \mathbf{F}_{p}^{-1}\Big|_{t} \left(\mathbf{I} - \mathbf{L}^{p} \Delta t\right), \tag{6}$$

where **I** is the second order identity tensor, and the subscript t+1 and t denote the current step and previous step, respectively. Δt is the time step increment. The updated plastic deformation gradient is used to calculate the elastic deformation gradient according to eqn.(1). The corresponding elastic Lagrangian strain \mathbf{E}_e can be obtained according to

$$\mathbf{E}_{e} = \frac{1}{2} \left(\mathbf{F}_{e}^{T} \mathbf{F}_{e} - \mathbf{I} \right). \tag{7}$$

The second Piola-Kirchhoff stress S, which represents the stress state in the deformed configuration is resolved by following the linear elastic relationship as

$$S = \mathbb{C} : E_{e} , \qquad (8)$$

where \mathbb{C} is the elasticity tensor. The above algorithms are implemented to the user subroutine UMAT in ABAQUS (Asaro and Rice, 1977; Hill and Rice, 1972; McGinty and McDowell, 2004; Peirce et al., 1982; Taylor, 1938).

Table 1 Summary of slip systems and slip strengths of crystalline phase in UHMWPE. Slip strengths are provided by Dong et al. (Dong et al., 2018).

Slip type	Slip system	Slip strength (GPa)	Illustration of slip activities			
Axial slip 1(a1)	(100)[001]	0.0698	Axial slip Transverse slip			
Axial slip 2 (a2)	(010)[001]	0.0912	(010)[001] (010)[100]			
Axial slip 3 (a3)	(110)[001]	0.1089				
Transverse slip 1 (t1)	(100)[010]	0.448				
Transverse slip 2 (t2)	(010)[100]	0.5006				
Transverse slip 3 (t3)	(110)[110]	0.2008	Kink bands Chain pull (001)[010] (001)[001]			
Kink bands 1 (k1)	(001)[100]	1				
Kink bands 2 (k2)	(001)[010]	1				
Chain pull (c1)	(001)[001]	6.3				

2.2 Macroscale constitutive modeling of the UHMWPE insert

Mechanical response of the UHMWPE insert at macro-scale is determined by homogenization of microscopic deformation. Based on the constitutive modeling in Section 2.1, the homogenized true stress-strain curve of each RVE is obtained through uniaxial compression simulation as shown in Fig. 2. A boundary velocity of 3 μ m/s is applied on one plane, while the opposite plane is fixed. Periodic boundary conditions are considered for the rest of the planes. Homogenized stress $\bar{\sigma}$ and strain $\bar{\varepsilon}$ are calculated through volume averaging of their microscopic counterparts over the RVE (Hill, 1967) as

$$\bar{\sigma} = \frac{1}{V} \int_{V} \sigma(1 + \varepsilon) dV$$
, and (9)

$$\overline{\varepsilon} = \frac{1}{V} \int_{V} \ln(1 + \varepsilon) dV. \tag{10}$$

Here, V is the volume of RVE. The homogenized stress-strain relationship is employed as the macroscopic material property of UHMWPE insert in the wear model as discussed in Section 2.3.

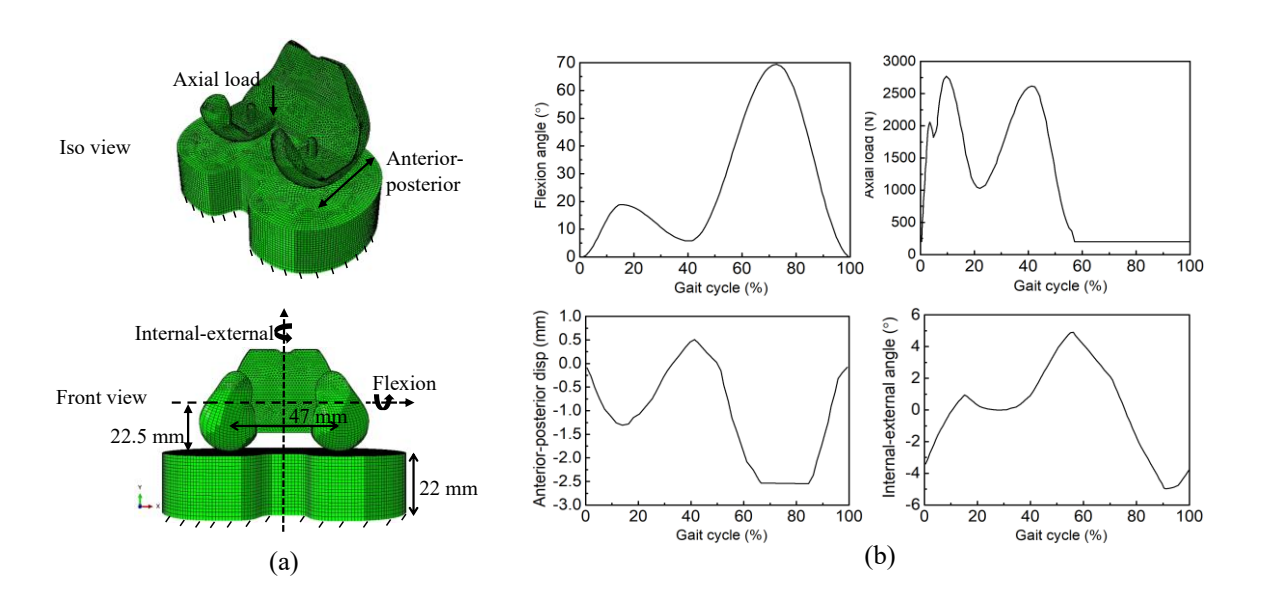


Fig. 4 (a) Wear model geometry and (b) external loadings history during a complete gait cycle (Abdelgaied et al., 2011).

2.3 Wear modeling of the of the UHMWPE insert

A finite element model as shown in Fig. 4(a) is developed to simulate the dynamic wear process using ABAQUS/Explicit. The femoral component is modeled as a rigid body that is subjected to combined axial load, anterior-posterior displacement, as well as flexion and internal-external rotations as shown in Fig. 4(b). Loading conditions follow the kinematic inputs from Abdelgaied et al. (Abdelgaied et al., 2011). Macroscale constitutive relationship of the flat UHMWPE insert is determined from Section 2.2. In this work, C3D8I element is selected for the insert part as this element type can remove shear locking and significantly reduce volumetric locking by supplementing the standard shape function with bubble functions that have a zero value at all nodes and non-zero values in between. The average mesh size of 1.3 mm is employed to ensure both computational efficiency and accuracy.

In this study, only abrasive wear is considered. Wear volume W is proportional to the contact area A and sliding distance S according to

$$W = CSA$$
 (Abdelgaied et al., 2011). (11)

Here, C is a non-dimensional and pressure independent wear coefficient. In the following analysis, $C = 10^{-9}$ is selected according to Abdelgaied et al. (Abdelgaied et al., 2011) and Kang et al. (Kang et al., 2008). Wear depth δ is employed to visualize the wear progression in the UHMWPE insert. Specifically, at a given time $t(0 \le t \le N)$, with N

being the total number of wear cycles), sliding distance associated with node i can be calculated as

$$S_i^t = \boldsymbol{U}_i^t \cdot \boldsymbol{n}_i^t , \qquad (12)$$

where U_i^t and n_i^t are the nodal displacement vector and unit tangent vector of the contact surface, respectively. Therefore, the accumulative wear depth δ_i^t is predicted according to

$$\delta_i^t = \sum_{t=0}^N CS_i^t . (13)$$

Wear rate \dot{W} of the entire UHMWPE insert is calculated as the total volume of removed materials divided by the number of wear cycles according to

$$\dot{W} = \sum_{i=1}^{M} \delta_i^t A_i^t / N , \qquad (14)$$

where M is the total node number on the insert contact surface, and A_i^t is the contact area associated with node i, respectively.

The computational model developed here can provide new physical insights of how microstructure affect the wear rate by resolving the microscopic deformation mechanisms. Systematic studies and discussions are provided in Section 3.

3. Results and discussion

According to Galvin et al. (Galvin et al., 2009), the experimentally measured wear rate of UHMWPE insert is 3.1 ± 1.3 mm³/million cycles under the same loading conditions as illustrated in Fig. 4. Microstructure information was not reported in their work. In the following computational studies, wear rate of UHMWPE insert is predicted by accounting for crystallinity, crystalline grain size and orientation. The microscopic deformation mechanisms are studied by looking at the load transfer behavior between the crystalline phase and amorphous phase, as well as the activation of different slip systems.

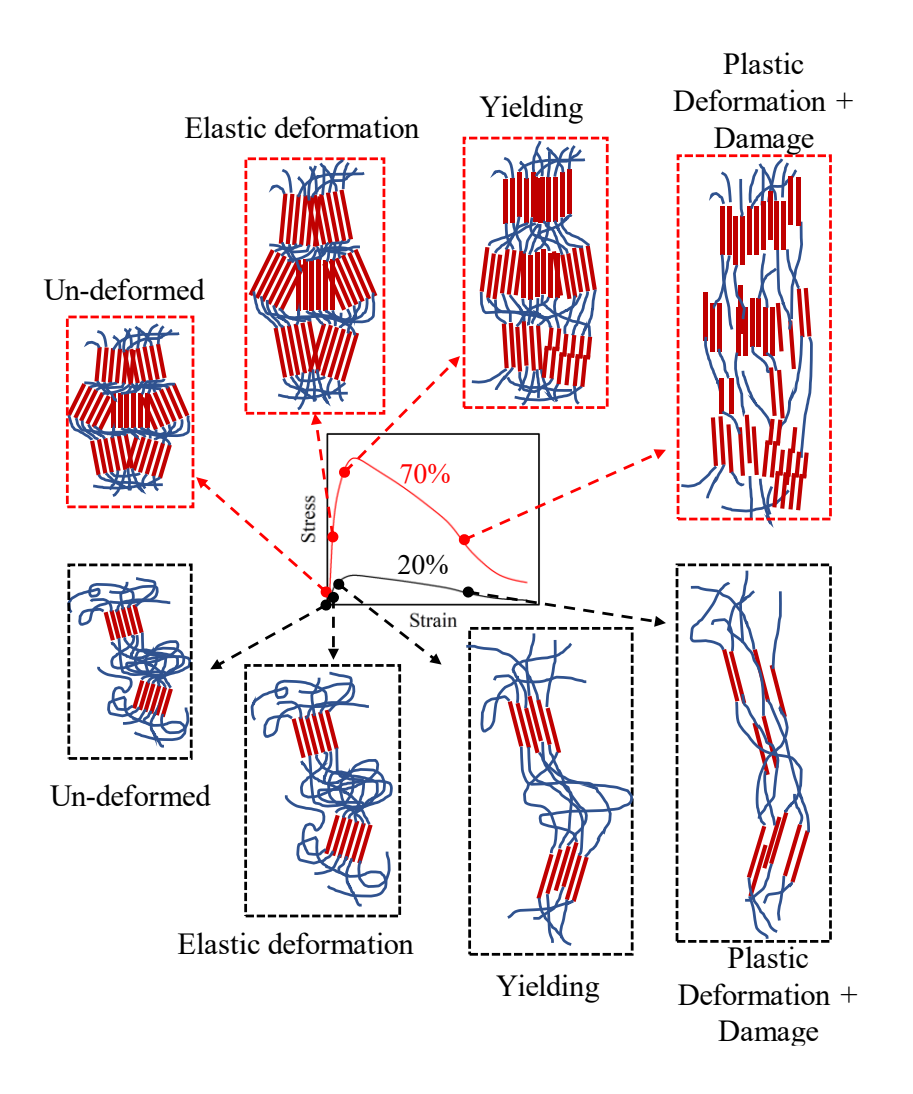


Fig. 5 Scheme of deformation in semi-crystalline polymers with low crystallinity (20%) and high crystallinity (70%), respectively.

3.1 Effect of crystallinity on wear behavior

During the course of uniaxial tension, deformation in semi-crystalline polymers usually starts from the amorphous phase. As illustrated in Fig. 5, initial elongation of the amorphous chains seldomly affect the orientation of crystalline lamellae. Further stretching in the axial direction leads to rotation and tilting of the lamellar crystals until they are aligned with the loading direction. No crystallographic slip is observed before the yield point. Plastic deformation involves dislocation motion induced unfolding in crystallites, as well as disentanglement and straightening in amorphous chains. Since slip activation in the crystalline phase is much harder than stretching and sliding in the amorphous phase, promoting plastic deformation in lamellar crystals can lead to higher material strength and stiffness. This can be achieved by increasing the crystallinity as illustrated in Fig. 5. In this set of study, RVEs in Fig. 3(a) with crystallinity of 20%, 40%, 50%, 60% and 70% are employed. These RVE samples share the same crystal grain size of 10 µm and follow

random orientation distributions. Five random RVE instantiations are considered under each crystallinity for statistical representation. According to Fig. 6, both yield strength and elastic modulus increase with crystallinity. The strengthening and stiffening effects become more obvious when crystallinity is beyond 60%. This is because at a dilute situation (e.g. crystallinity is 20%), very limited crystalline grains can share the applied load. Excessive slip can unfold the crystalline phase and eventually turn the highly ordered chain structures to the amorphous state. Increasing crystallinity can help mitigate the load by avoiding severe local deformation, therefore, leading to higher strength and stiffness. From our wear simulation results, the increase in crystallinity also results in a measurable improvement in wear resistance. As illustrated in Fig. 7(a), wear rate decreases from 3.25 mm³/million cycles to 2.38 mm³/million cycles when crystallinity increases from 20% to 70%. The same trend was also found experimentally by Karuppiah et al. (Kanaga Karuppiah et al., 2008) through nanoindentation as the wear resistance tends to be higher in regions with more pronounced lamellae structure than in less pronounced regions. The simulated wear patterns in Fig. 7(b) are very similar to the experimental observation from Galvin et al. (Galvin et al., 2009). It should be noted that the existing manufacturing approach can only fabricate UHMWPE with crystallinity up to around 70%. This is because when an amorphous polymer is cooled, crystallization occurs at a temperature depending on the rate of cooling. Due to the crystallization kinetics, crystallization ceases long before the amorphous phase completes the conversion process. Therefore, there is a limit in improving the wear resistance by increasing crystallinity alone.

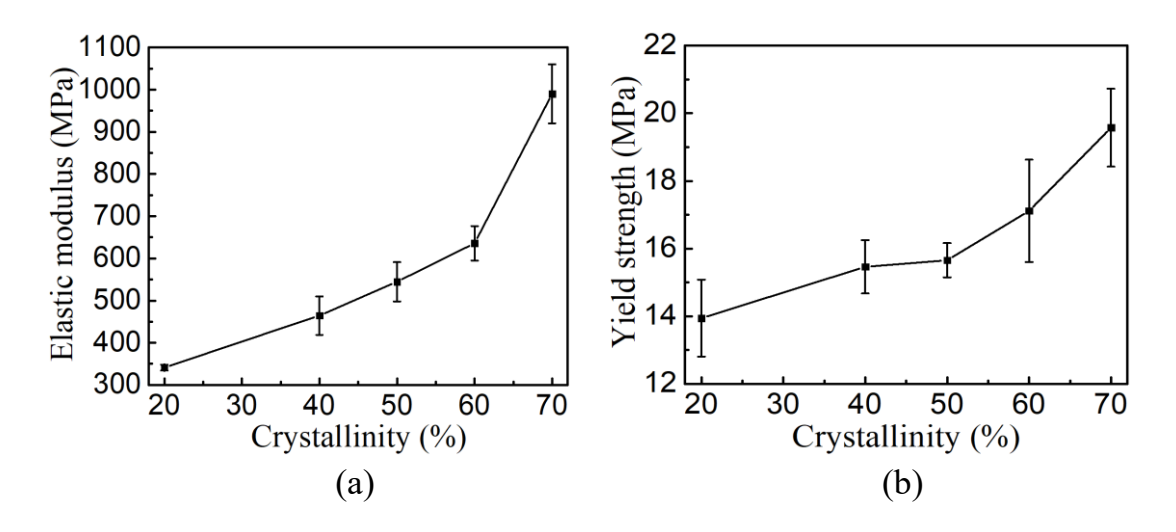


Fig. 6 Effect of crystallinity on (a) elastic modulus and (b) yield strength.

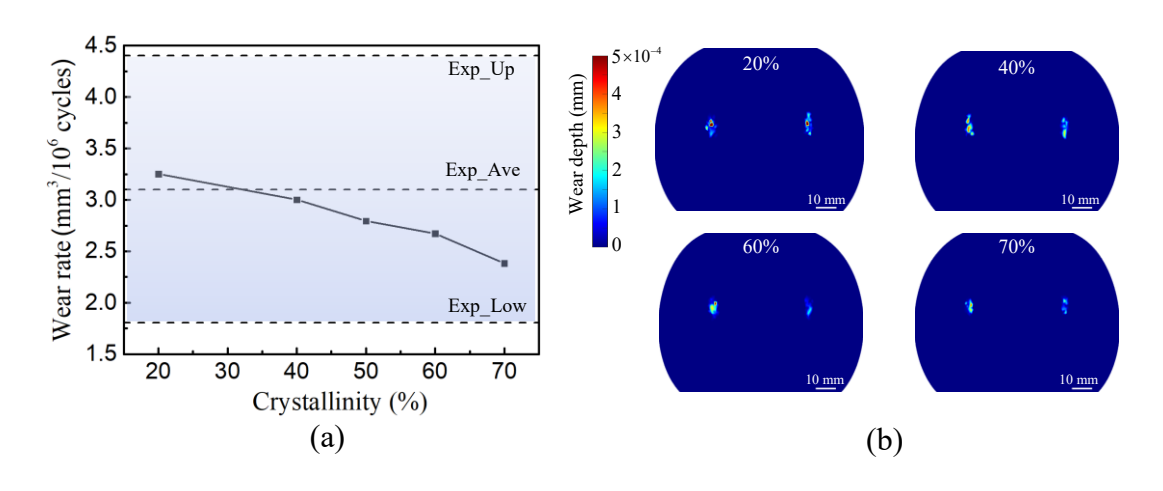


Fig 7. Effect of crystallinity on (a) wear rate, and (b) wear patterns.

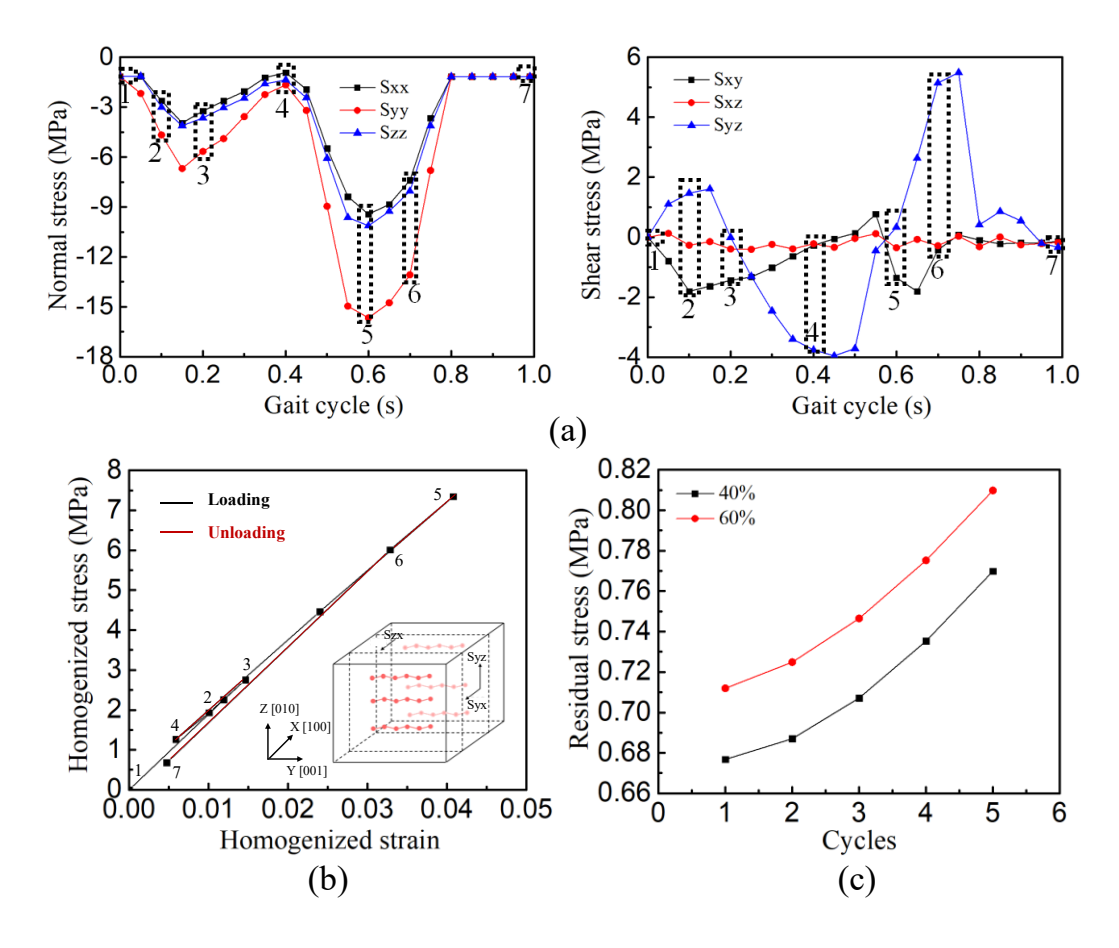


Fig. 8 (a) Stress state at the initiation wear site during the first wear cycle, (b) equivalent stress-strain response of the RVE (40% crystallinity with crystal size of 10 μm) by applying the extracted stress state from (a) as loading conditions, and (c) effect of crystallinity on residual stress during different wear cycles. All the crystal grains in the RVE are orientated in the Y direction [001].

From the macroscale wear simulation, stress state at the first observed wear site is extracted and applied back to the corresponding RVE as loading conditions. Fig. 8(a) demonstrates the extracted stress state in one case with 40% crystallinity and 10 µm crystal grain size. In order to eliminate the effect of chain orientation in this set of study, all the crystal grains in the RVE are orientated in the Y direction [001] as illustrated in Fig 8(b). The equivalent stress-strain response of RVE during the first wear cycle is shown in Fig. 8(b). It is noted that plastic deformation occurs at point 2 before the first unloading event starts at point 3. Hysteresis behavior is observed in the subsequent reloading and unloading processes. A residual stress of 0.68 MPa is observed at point 7 after the first wear cycle. It is found from Fig. 8(c) that residual stress increases with the number of wear cycles. This cumulative effect can accelerate the wear process in the UHMWPE insert. Increasing crystallinity, although can effectively improves material strength, would also lead to more intensive residual stress under wear loading. It can be concluded that analysis from simple tension/compression cannot provide sufficient information in understanding the complex deformation and wear mechanisms in UHMWPE. In order to quantitatively compare the material response under both uniaxial loading and wear loading, we extract the maximum principal stress from the loading conditions in Fig. 8(a) and apply it to the Y direction [001] and Z direction [010] of each RVE, respectively. This represents a more exaggerated uniaxial loading condition that the RVEs would experience. It can be seen from Fig. 9 that transverse slip is the dominant deformation mechanism in the crystalline phase when the maximum principal stress is applied along the chain direction (Y direction). No slip system is activated when the same load is applied to the transverse direction (Z direction). When the RVE is subjected to wear loading, the resolved plastic strain on the transverse slip systems tends to saturate at a plateau during the first wear cycle. A higher plateau is achieved in the next wear cycle with a similar pattern. During the first cycle, the maximum resolved plastic strain that can be achieved under uniaxial loading is 66.6% lower than that under the wear loading when crystallinity is 40%, according to Fig. 9(c). The difference between the two resolved plastic strains is reduced to 31.9% when crystallinity increases to 60%. This indicates that uniaxial test would underestimate the plastic deformation in UHMWPE, especially when crystallinity is low. Since plastic deformation is the primary driving force for wear formation, material response from uniaxial test can lead to a lower wear rate prediction. This is another reason why the UHMWPE insert may fail sooner than expected. Microscale analysis can provide interesting new perspectives that have not been discussed yet. For example, plastic deformation in the crystalline phase can be triggered when the entire RVE undergoes unloading. As shown in Fig. 9(c), transverse slip is activated around 0.6 s and saturated at the first plateau at 0.8 s when crystallinity is 40%. This corresponds to part of the unloading period from point 5 to point 6 in Fig. 8(b). The seemingly counter-intuitive result can be explained by taking a closer look at the interplay between the crystalline and amorphous phases. Before transverse slip is activated in the crystalline phase at 0.6 s, plastic deformation has already been initiated in the amorphous phase since 0.4 s, as indicated in Fig. 10. There is a rapid increase of plastic deformation in the amorphous phase from 0.5 s to 0.6 s, followed by a plateau due to the unloading behavior in the entire RVE. It should be noted that the shear components do not follow the same pattern as the normal components. As illustrated in Fig. 8(a), shear load S_{yz} keeps increasing from 0.33 MPa at 0.6 s to 5.16 MPa at 0.75 s, while the corresponding normal loads decrease to zero. Under the same shear loading, resolved plastic strain along the transverse slip direction can be 10^{11} times larger when crystallinity increases from 40% to 60% according to Fig. 9(c). This responds to an average 4.41% increase in residual stress after complete unloading process in each cycle as shown in Fig. 8(c). It is worth noting that both the resolved plastic strain and residual stress are very low initially. However, they keep building up on the contact surface and eventually cause detrimental wear damages after millions of cycles.

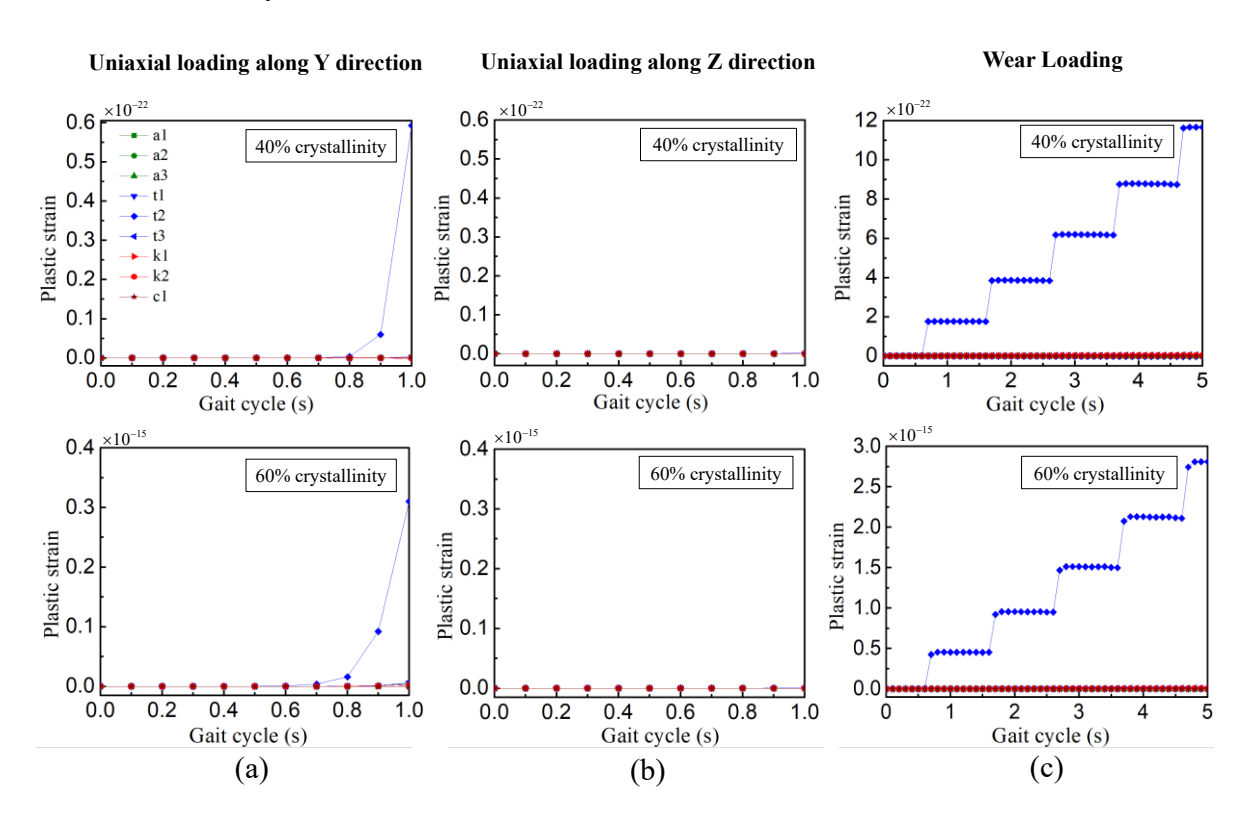


Fig. 9 Resolved plastic strain on slip systems under uniaxial loading in (a) Y direction [001], (b) Z direction [010], and (c) wear loading condition in RVEs with 40% and 60% crystallinity, respectively.

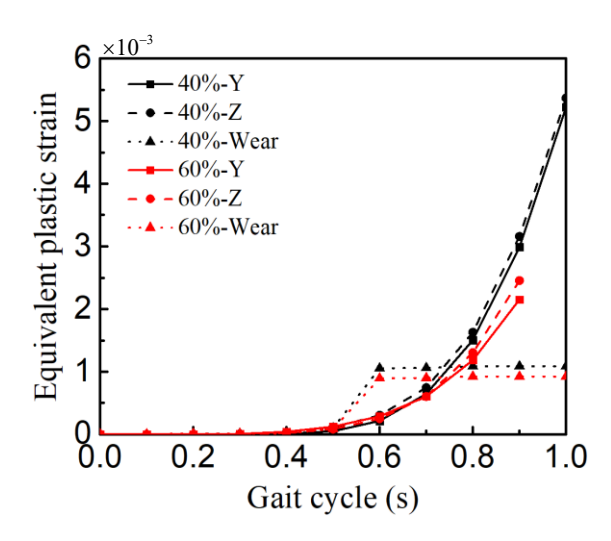


Fig. 10 Equivalent plastic strain evolution in amorphous phase of RVEs with 40% and 60% crystallinity. Uniaxial loading in Y direction [001] and Z direction [010], as well as wear loading are considered.

3.2 Effect of crystal orientation on wear behavior

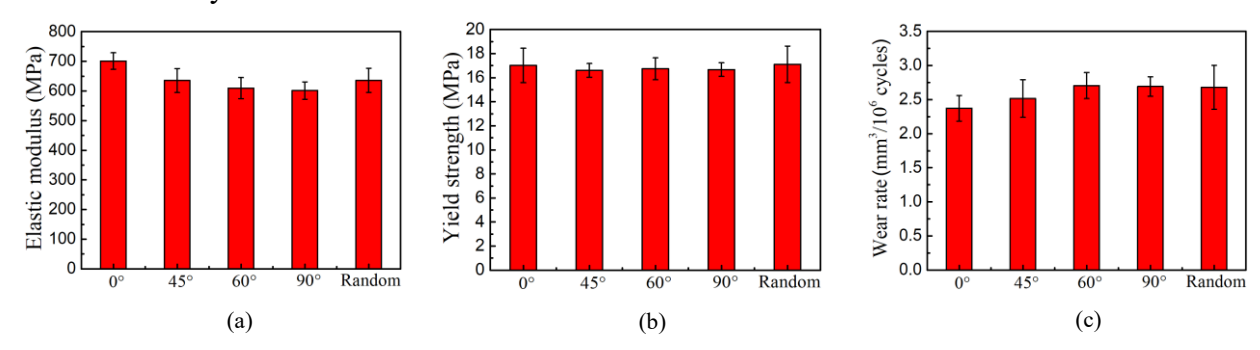


Fig. 11 Effect of crystal grain orientation on (a) elastic modulus, (b) yield strength and (c) wear rate.

In this set of study, RVE samples with 60% crystallinity and 10 μ m crystal grains are employed. Crystal grains follow 0°, 45°, 60°, 90° and random orientations as shown in Fig. 3(b). It is noted from Fig. 11(a) that RVEs with chains aligned with the uniaxial loading direction (0° case) exhibit the highest elastic modulus. Increasing the angle between chain orientation and loading direction can result in decreased material stiffness due to the intensified crystal grain reorientation. Yield strength, on the other hand, is much less affected by crystal grain orientation than crystallinity according to Fig. 11(b). It should be noted that evaluation of elastic modulus and yield strength from uniaxial loading simulations cannot lead to direct prediction of wear rate when the RVEs are subjected to more complex wear loading condition as illustrated in Fig. 8(a). As shown in Fig. 11(c), wear rate only slightly increases when the crystal grains are oriented from 0° to 60°, but starts to saturate upon further tilting to 90°. When crystal grain orientations are randomly

assigned in the RVE, the corresponding wear rate does not fall between the predictions of 0° and 90° scenarios like the elastic modulus and yield strength that are extracted from uniaxial tension tests. Instead, the average wear rate under random orientation is very close to the highest wear rate value, indicating that direct knowledge transfer from uniaxial simulation can overestimate the wear resistance in UHMWPE insert. This finding resonates with our discussions in Section 3.1 and the observations from other researchers (Abdelgaied et al., 2011; Zhang et al., 2017).

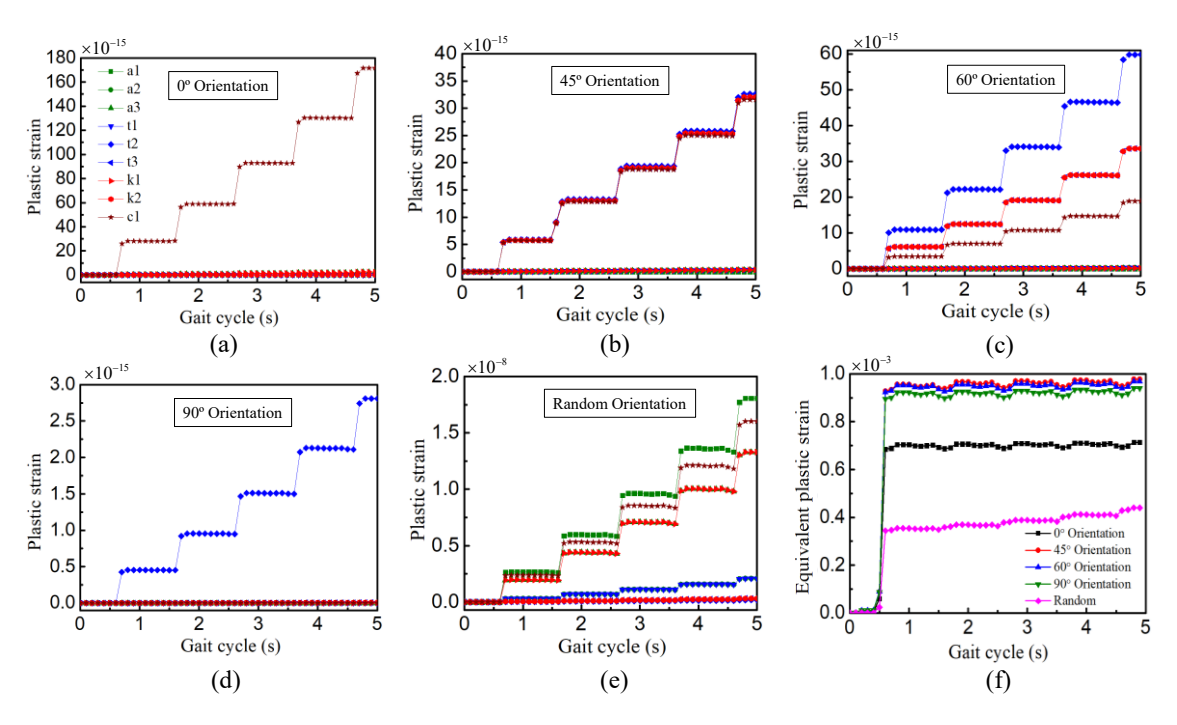


Fig. 12 Resolved plastic strain on slip systems in RVEs with (a) 0°, (b) 45°, (c) 60°, (d) 90° and (e) random crystal grain orientations under wear loading conditions. (f) Equivalent plastic strain in amorphous phase under different crystal grain orientations.

It is noted from the analysis in Fig. 12 that when crystal grains are orientation along the 0° direction, chain pull is the only activated slip system. As the orientation angles increases, transverse slip and kink bands gradually emerge. According to Table 1, the slip strength required to activate the chain pull system is 6.3 times greater than the kink band systems, 14 to 31.37 times greater than the transverse systems and 57.85 to 90.26 times greater than the axial slip systems, respectively. Therefore, activation of chain pull system with the highest plastic strain can effectively mitigate the load from the amorphous phase to the crystalline phase according to Fig. 12(f), leading to improved wear resistance. It is interesting to notice that a more pronounced plastic deformation is observed in the crystalline phase when crystal grains follow random orientations. The corresponding equivalent plastic strain in the amorphous phase is reduced by half compared to the 0° case scenario. However, the wear rate is not reduced accordingly. There could be several reasons for this result. Firstly, plastic deformation allows wear to continue indefinitely both

in depth and extent (Hu et al., 2016). Although mitigating plastic deformation from the amorphous phase to the crystalline phase can help improve the wear resistance, this trend does not hold if the plastic deformation in the crystalline phase exceeds a certain threshold. For example, when crystal grain orientation decreases from 45° to 0°, the overall plastic strain in the crystalline phase is almost tripled, leading to 5% decrease in wear rate. When crystalline grains are randomly oriented, plastic deformation in crystalline phase becomes seven orders of magnitude higher than the monotonic orientation cases. The excessive plastic deformation negatively affects the wear resistance according to Fig. 11(c). Secondly, axial slip, which requires the lowest slip strength to activate, is the dominant deformation mechanism in the random orientation case. It ultimately results in higher overall plastic deformation under the same wear loading conditions. Additionally, more slip systems can be activated simultaneously when random grain orientation is applied. This makes plastic deformation easier to occur, and therefore accelerating the wear process. From the manufacturing perspective, it is impossible to align the crystalline chain in a monotonic direction. According to the above case studies, the wear resistance can be improved if the texture of UHMWPE insert can primarily align with the axial load direction as illustrated in Fig. 4(a).

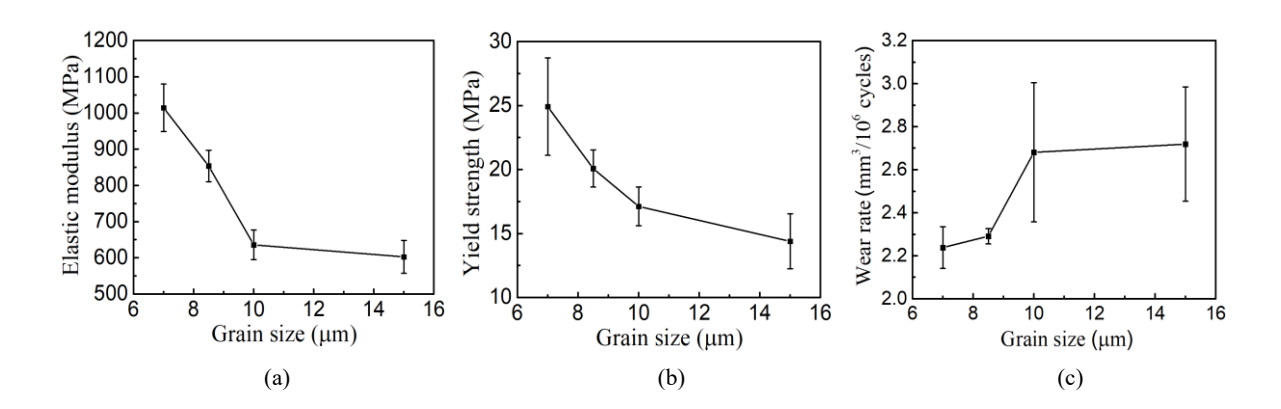


Fig. 13 Effect of crystal grain size on (a) elastic modulus, (b) yield strength and (c) wear rate.

3.3 Effect of crystal grain size on wear behavior

The forgoing parametric studies all consider RVEs with a constant crystal grain size (grain diameter) of 10 μ m. In the following simulations, RVEs with 60% crystallinity and grain size of 7 μ m, 8.5 μ m, 10 μ m and 15 μ m are considered, respectively. Crystal grains follow random orientations.

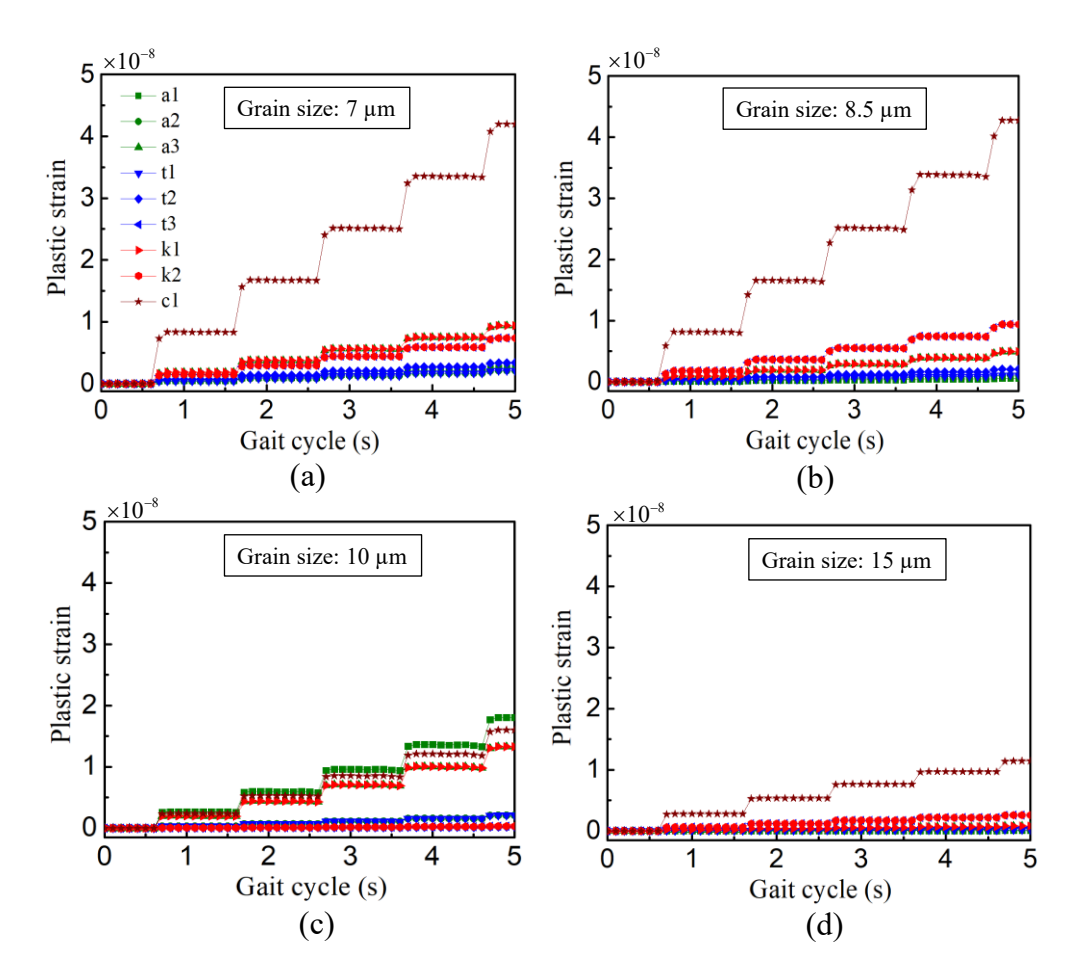


Fig. 14 Resolved plastic strain on slip systems in RVEs with grain size of (a) 7 μ m, (b) 8.5 μ m, (c) 10 μ m, and (d) 15 μ m, respectively. RVEs have 60% crystallinity with random grain orientations.

As shown in Fig. 13, increasing grain size negatively affect the stiffness, strength and wear resistance. In order to find the correlation between wear rate and microscale deformation mechanisms, we conduct slip system analysis based on a set of RVEs that share the same spatial distribution of grain centroids, but with different grain sizes. It can be seen from Fig. 14 that reducing grain size can promote activation of chain pull slip, which is a beneficial deformation mechanism for improving the wear resistance. Additionally, smaller crystal grains can effectively alleviate the plastic deformation in the amorphous phase. As shown in Fig. 15, there is approximately 80% decrease in plastic strain in the amorphous phase when grain size is reduced from 15 µm to 7 µm. Ideally, if the crystalline phase can accommodate the entire load without triggering deformation in the amorphous phase, the corresponding wear resistance would be significantly improved. However, in real case scenarios, it is nearly impossible to allocate all the deformation to the crystalline phase. A more realistic design approach is to redistribute the deformation so that the crystalline phase can take a higher share of the external load. It is noted from Fig. 16 that smaller crystalline grains are more effective in load sharing than large grains. When grain

size increases, high stress tends to transfer from the crystalline phase to the crystalline/amorphous interface. Reduced load sharing in the crystalline phase ultimately results in decreased material stiffness, strength and wear resistance. It is also worth remarking that large crystal grains can cause greater uncertainty in wear resistance than stiffness and strength. As indicated in Fig 13(c), a larger scatter of wear rate is predicted when the grain size is above 8.5 µm. This is because material deformation under wear loading conditions tends to be more localized. With the same crystallinity, fewer crystal grains exist when the size increases. In an extreme case where no crystalline grain is near the contact surface, wear damage can easily initiate and in turn accelerate the failure of the entire implant device. This phenomenon becomes more prominent when crystallinity is low.

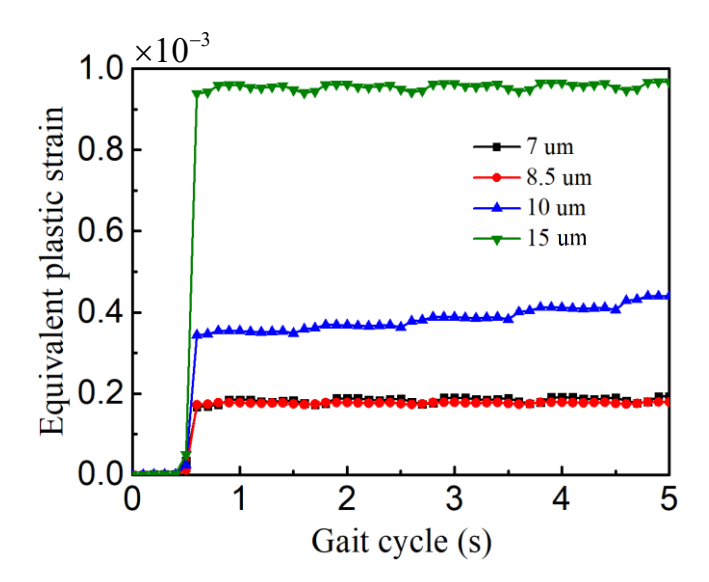


Fig. 15 Equivalent plastic strain in the amorphous phase of RVEs with different crystal grain size.

It can be concluded from the forgoing analysis that wear damage in UHMWPE insert essentially depends on the interplay of plastic deformation between the crystalline phase and amorphous phase, as well as the detailed microscale deformation mechanisms in the crystalline phase. First of all, improving wear resistance requires reducing the overall plastic deformation upon the same kinematic inputs. This can be achieved by promoting load bearing capacity in the crystalline phase through increased crystallinity and decreased crystal grain size. Manufacturing techniques that can prevent crystalline phase aggregation in UHMWPE would enhance both the wear resistance and reliability. Besides, texture alignment along the axial load direction can help improve the wear resistance by triggering chain pull slip when the crystalline phase undergoes plastic deformation.

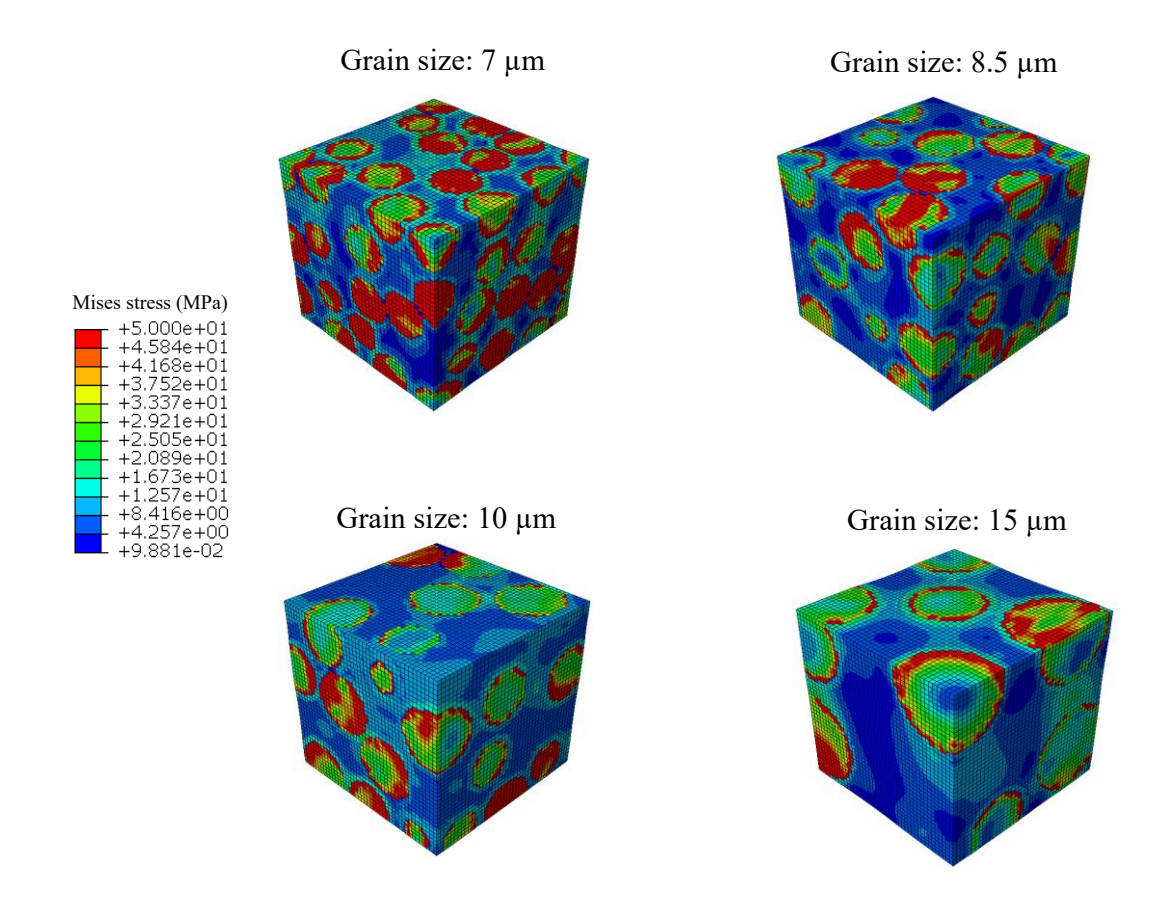


Fig. 16 Stress distribution in UHMWPE RVEs with different crystalline grain sizes. All the RVEs have 60% crystallinity and follow random grain orientations.

5. Conclusions

A multiscale computational framework, which predicts the wear rate of UHMWPE insert by explicitly accounting for detailed microstructure attributes, such as crystallinity, crystal grain orientation and size, is presented. At the macroscale level, dynamic wear process is simulated using ABAQUS/Explicit by applying realistic kinematic input measured from wear tests. Wear rate is predicted by calculating the wear volume per cumulative cycles. Evolution of stress is extracted from the initial wear site and applied back to the UHMWPE microstructure as loading conditions. At the microscale level, a semi-crystal plasticity model is developed to resolve the heterogeneous deformation. Activation of different slip systems and its role on wear resistance are systematically studied. The new physical insights we found from this study are summarized below:

1. Material properties measured from uniaxial tension test cannot be directly used to evaluate the wear resistance. Under more complex dynamic and cyclic loading conditions, the actual wear rate of UHMWPE insert is usually higher than the numerical prediction if microstructure-induced heterogenous deformation is not taken into account.

- 2. The fundamental avenue for improving the wear resistance of UHMWPE insert is to minimize the total plastic deformation upon the same external loading. In general, increasing crystallinity and decreasing crystal grain size can promote load transfer from the amorphous phase to the crystalline phase, leading to improved wear performance.
- 3. Plastic deformation in the crystalline phase, although alleviates stretching and damage in the amorphous phase, can negatively impact the overall material strength and wear resistance if its plastic strain exceeds a certain threshold. Activation of chain pull slip other than multiple slip systems can help improving the wear resistance. Texture alignment along the axial load direction can promote this beneficial deformation mechanism.

The capability of this multiscale framework can be further extended to address crystalline grain tilting and unfolding during the wear process. This effort requires updating the crystal grain orientation and macroscale stress-strain response after each step. The computational cost can be very expensive if the actual wear cycles in 10 to 15 years are considered. Integration of machine learning in wear simulations could be a promising way to address this challenge and provide useful material selection and geometry design guidance based on different patients' needs. Similar work on cross-scale property prediction in metals using machine learning technique has been reported (Sun et al., 2021).

CRediT authorship contribution statement

Yan Li: Conceptualization, Methodology, Data analysis, Writing, and Supervision.

Chi Ma: Software, Data curation and Visualization.

Declaration of Competing Interest

The authors declare that they have no known competing financial interests or personal relationships that could have appeared to influence the work reported in this paper.

Acknowledgement

The authors acknowledge the support from NH BioMade Project which is provided by the National Science Foundation's Research Infrastructure Improvement Award # 1757371, as well as the start-up funds from Thayer School of Engineering at Dartmouth College. The authors also acknowledge the insightful discussions with Professor Doug Van Citters and the SOLIDWORKS modeling guidance from Joseph N. Poissant at Thayer School of Engineering.

References

Abdelgaied, A., Liu, F., Brockett, C., Jennings, L., Fisher, J., Jin, Z., 2011. Computational wear prediction of artificial knee joints based on a new wear law and formulation. Journal of biomechanics 44, 1108-1116.

Asaro, R.J., Rice, J.R., 1977. Strain Localization in Ductile Single-Crystals. J Mech Phys Solids 25, 309-338.

Becker, J.S., Brown, R.D., Killelea, D.R., Yuan, H., Sibener, S.J., 2011. Comparative surface dynamics of amorphous and semicrystalline polymer films. Proceedings of the National Academy of Sciences 108, 977-982.

Bowden, P.B., Young, R.J., 1974. Deformation mechanisms in crystalline polymers. Journal of Materials Science 9, 2034-2051.

Callaghan, J.J., O'Rourke, M.R., Saleh, K.J., 2004. Why knees fail: Lessons learned1 1Benefits or funds were received in partial or total support of the research material described in this article from DePuy, Warsaw, IN and Zimmer, Warsaw, IN. The Journal of Arthroplasty 19, 31-34.

Carr, B.C., Goswami, T., 2009. Knee implants—review of models and biomechanics. Materials & Design 30, 398-413.

Dong, H., Wang, Z., O'Connor, T.C., Azoug, A., Robbins, M.O., Nguyen, T.D., 2018. Micromechanical models for the stiffness and strength of UHMWPE macrofibrils. Journal of the Mechanics and Physics of Solids 116, 70-98.

Galvin, A.L., Kang, L., Udofia, I., Jennings, L.M., McEwen, H.M.J., Jin, Z., Fisher, J., 2009. Effect of conformity and contact stress on wear in fixed-bearing total knee prostheses. Journal of Biomechanics 42, 1898-1902.

Godest, A.C., Beaugonin, M., Haug, E., Taylor, M., Gregson, P.J., 2002. Simulation of a knee joint replacement during a gait cycle using explicit finite element analysis. Journal of Biomechanics 35, 267-275.

Hill, R., 1967. The essential structure of constitutive laws for metal composites and polycrystals. Journal of the Mechanics and Physics of Solids 15, 79-95.

Hill, R., Rice, J.R., 1972. Constitutive analysis of elastic-plastic crystals at arbitrary strain. J Mech Phys Solids 20, 401-413.

Hu, Z., Lu, W., Thouless, M.D., Barber, J.R., 2016. Effect of plastic deformation on the evolution of wear and local stress fields in fretting. International Journal of Solids and Structures 82, 1-8.

Ishikawa, H., Fujiki, H., Yasuda, K., 1996. Contact Analysis of Ultrahigh Molecular Weight Polyethylene Articular Plate in Artificial Knee Joint During Gait Movement. Journal of Biomechanical Engineering 118, 377-386.

Kanaga Karuppiah, K.S., Bruck, A.L., Sundararajan, S., Wang, J., Lin, Z., Xu, Z.-H., Li, X., 2008. Friction and wear behavior of ultra-high molecular weight polyethylene as a function of polymer crystallinity. Acta Biomaterialia 4, 1401-1410.

- Kang, L., Galvin, A.L., Brown, T.D., Jin, Z., Fisher, J., 2008. Quantification of the effect of cross-shear on the wear of conventional and highly cross-linked UHMWPE. Journal of biomechanics 41, 340-346.
- Knight, L.A., Pal, S., Coleman, J.C., Bronson, F., Haider, H., Levine, D.L., Taylor, M., Rullkoetter, P.J., 2007. Comparison of long-term numerical and experimental total knee replacement wear during simulated gait loading. Journal of biomechanics 40, 1550-1558.
- Lee, B.J., Parks, D.M., Ahzi, S., 1993. Micromechanical modeling of large plastic deformation and texture evolution in semi-crystalline polymers. Journal of the Mechanics and Physics of Solids 41, 1651-1687.
- Lin, L., Argon, A.S., 1994. Structure and plastic deformation of polyethylene. Journal of Materials Science 29, 294-323.
- McEwen, H.M., Barnett, P.I., Bell, C.J., Farrar, R., Auger, D.D., Stone, M.H., Fisher, J., 2005. The influence of design, materials and kinematics on the in vitro wear of total knee replacements. J Biomech 38, 357-365.
- McGinty, R.D., McDowell, D.L., 2004. Application of multiscale crystal plasticity models to forming limit diagrams. J Eng Mater-T Asme 126, 285-291.
- Nich, C., Goodman, S.B., 2014. Role of macrophages in the biological reaction to wear debris from joint replacements. Journal of long-term effects of medical implants 24, 259-265.
- Peirce, D., Asaro, R.J., Needleman, A., 1982. An Analysis of Nonuniform and Localized Deformation in Ductile Single-Crystals. Acta Metallurgica 30, 1087-1119.
- Polińska, M., Rozanski, A., Galeski, A., Bojda, J., 2021. The Modulus of the Amorphous Phase of Semicrystalline Polymers. Macromolecules 54, 9113-9123.
- Sanders, A.P., Lockard, C.A., Weisenburger, J.N., Haider, H., Raeymaekers, B., 2016. Using a surrogate contact pair to evaluate polyethylene wear in prosthetic knee joints. Journal of Biomedical Materials Research Part B: Applied Biomaterials 104, 133-140.
- Sathasivam, S., Walker, P.S., 1997. A computer model with surface friction for the prediction of total knee kinematics. Journal of Biomechanics 30, 177-184.
- Sun, X., Li, H., Zhan, M., Zhou, J., Zhang, J., Gao, J., 2021. Cross-scale prediction from RVE to component. International Journal of Plasticity 140, 102973.
- Suñer, S., Tipper, J.L., Emami, N., 2012. Biological effects of wear particles generated in total joint replacements: trends and future prospects. Tribology Materials, Surfaces & Interfaces 6, 39-52.
- Taylor, G.I., 1938. Plastic strain in metals. J I Met 62, 307-324.
- Van Dommelen, J.A.W.v., Parks, D.M., Boyce, M.C., Brekelmans, W.A.M., Baaijens, F.P.T., 2003. Micromechanical modeling of the elasto-viscoplastic behavior of semi-crystalline polymers. Journal of the Mechanics and Physics of Solids 51, 519-541.
- Zhang, J., Chen, Z., Wang, L., Li, D., Jin, Z., 2017. A patient-specific wear prediction framework for an artificial knee joint with coupled musculoskeletal multibody-dynamics and finite element analysis. Tribology International 109, 382-389.